2025 IEEE International Conference on Metrology for eXtended Reality, Artificial Intelligence and Neural Engineering (MetroXRAINE) | 979-8-3315-0279-9/25/$31.00 ©2025 IEEE | DOI: 10.1109/METROXRAINE66377.2025.11340013

Investigation of the Relationship between High and Low Frequency Resistances of Li-ion Batteries: A Machine Learning Approach

Simone Barcellona*, Loris Cannelli†, Lorenzo Codecasa*, Silvia Colnago‡, Loredana Cristaldi*, Christian Laurano* and Gabriele Maroni†
*DEIB, Politecnico di Milano, Milano, Italy
†IDSIA, SUPSI-USI, Lugano, Switzerland
‡TGM, Ricerca sul Sistema Energetico S.p.A., Milano, Italy

***Abstract*—Lithium-ion batteries (LiBs) are widely used in diverse applications due to their high energy and power density, efficiency, and long cycle life. However, their performance varies over time due to a combination of reversible effects and irreversible aging mechanisms, driven by factors such as temperature, state of charge (SOC), and current rate. Accurate estimation of key battery parameters—including internal resistance—is essential for assessing the state of health (SOH), SOC, and state of power, which are critical for reliable operation and battery management. This work proposes a machine learning approach for estimating the low-frequency internal resistance of LiBs, leveraging prior estimation of the high-frequency component. The method builds on previous research and aims to provide accurate predictions across varying SOC, temperature, and aging conditions, while avoiding the need for complex hardware or intensive computations. The results show that, although estimating low-frequency resistance is inherently challenging, the use of a neural network—especially when incorporating high-frequency resistance as an input—reduces the estimation error to below 3%. The proposed model represents a promising solution for practical, real-time resistance estimation in advanced battery management systems.**

I. Introduction

Among rechargeable batteries, lithium-ion batteries (LiBs) are widely used across a broad range of applications such as smartphones, notebooks, medical tools, electric vehicles, and stationary systems supporting renewable energy sources [1]. This widespread use of LiBs is driven by their strong performance characteristics, including high energy and power density, high coulombic and energy efficiency, low self-discharge rates, relatively long lifetime, and no memory effect [2]. Especially in transportation applications, both the energy and power a battery can deliver are crucial to ensure long service life and optimal dynamic performance.

Nevertheless, LiBs are subject to various aging mechanisms, both during storage and use. For instance, depending on the temperature and state of charge (SOC) at which the battery is stored, the aging rate can accelerate or decelerate (calendar aging) over time. Similarly, during operation, factors such as temperature, SOC, current rate, SOC window, and voltage limits influence the battery degradation (cycle aging) as a function of number of cycles or total charge throughput (referred to as moved charge) [3].

Therefore, the optimal way to use or store the battery can improve its efficiency and reduce the aging rate. In any case, battery degradation primarily leads to two consequences: a decrease in the ability to store energy (energy fade) and a decrease in the ability to deliver electrical power (power fade). While the former depends on the battery capacity, the latter is related to its internal resistance. For this reason, both capacity loss and resistance increase are commonly used as indicators of the state of health (SOH) of LiBs [4].

In addition to SOH estimation, other battery states such as SOC and state of power (SOP) are essential for determining the remaining capacity and available power of the battery [5]. Therefore, accurate estimation of these parameters is critical for diagnostics, prognostics, and ensuring the optimal and safe operation of the battery.

Besides the irreversible changes in both battery capacity and internal resistance caused by degradation, the same factors that influence the aging rate (such as temperature, SOC, current rate, etc.) also have a reversible effect on the actual values of capacity or resistance [6], [7].

Focusing on SOP and power fade, this work aims to analyze the estimation of the battery internal resistance under various conditions. Several studies in the literature have analyzed how internal resistance varies reversibly with SOC or battery temperature [8], [9]. Conversely, other studies have examined how different SOC and temperature conditions affect both calendar and cycle aging, leading to an increase in internal resistance [10], [11]. A more comprehensive analysis was presented in a previous work [12], in which the authors investigated the combined reversible and irreversible effects of various SOC and temperature conditions on internal resistance in different aging states.

Regarding the estimation methods for battery internal resistance, while various classifications exist in the literature, in this work, we primarily categorize them into non-model-based and model-based approaches. In this regard, it is important to

The work of Silvia Colnago has been financed by the Research Fund for the Italian Electrical System under the Three-Year Research Plan 2022-2024 (DM MITE n. 337, 15.09.2022), in compliance with the Decree of April 16th, 2018

note that the internal resistance of a LiB consists of multiple components [13]. Specifically, it can be divided into a high-frequency term and a low-frequency term, as further discussed in the next section.

Non-model-based methods rely on direct measurements and can be further divided into time-domain and frequency-domain techniques. Among the time-domain methods, the most frequently used is the dc current pulse method. This approach involves applying a current pulse to the battery under test and observing the resulting change in voltage over a defined time interval [14]. In the frequency domain, electrochemical impedance spectroscopy (EIS) is a well-established technique. It works by applying a small sinusoidal current (galvanostatic EIS, GEIS) or voltage (potentiostatic EIS) at multiple frequencies and measuring the corresponding voltage or current response [15]. Through this process, it is possible to characterize the impedance of the battery across a wide range of frequencies. These methods can achieve high accuracy but may be difficult to implement for online and real-time applications.

On the other hand, model-based methods encompass a wide range of approaches, which can be broadly categorized into physics-based models, data-driven approaches, and hybrid methods that combine elements of both [16]. Physics-based models, although computationally demanding, offer high accuracy by providing a detailed description of the electrochemical and physical processes occurring within the battery [17], [18]. In contrast, data-driven approaches are typically simpler but may be less accurate. They often rely on analytical functions fitted to experimental data, or, more recently, on machine learning (ML) techniques that learn patterns from data without requiring explicit physical knowledge of the system [19]–[21].

Although the internal resistance of a battery can serve as an SOH indicator for power fade, most works in the literature focus primarily on SOH estimation in terms of capacity fade. In some of these studies, internal resistance is used either as part of the battery model or as a feature for ML models. Specifically, in ML-based approaches, internal resistance is often estimated using other algorithms, such as the Kalman filter and their derivative algorithms or recursive least squares, and the estimated resistance is then fed as an input feature to the ML model [22]–[24]. However, studies that attempt direct estimation of internal resistance using ML techniques appear to be scarce in the literature.

Specifically, in [25], the authors employed an ML approach involving two neural networks (NNs). The first NN estimated the battery capacity based on voltage, current, and temperature, while the second NN estimated the internal resistance—specifically the solid electrolyte interface (SEI) and charge transfer resistance—using both the same inputs as the first NN and its estimated capacity output. On the other hand, a previous work [15], proposed a simple ML approach to estimate the high-frequency resistance of a LiB under different conditions of SOC, temperature, and aging levels, without using battery capacity as a feature. In particular, the proposed approach showed promising results in estimating resistance variations at unknown SOC levels and under future aging conditions, despite relying on a limited dataset with few features and without the need for resource-intensive computational tools.

Moreover, while the high-frequency resistance can be relatively easily estimated online using non-model-based methods—such as by superimposing a high-frequency signal through the existing power converter used for battery operation—the low-frequency resistance is more challenging to estimate with these techniques.

In the present work, an ML approach similar to [15] was developed to estimate the low-frequency resistance of the same type of LiB, based on the estimation of the high-frequency resistance.

II. Electrical model and Experimental Activity

The battery internal resistance is composed of four different contributions [13]. Specifically, it can be decomposed into a high-frequency term related to the ohmic resistance of the materials that make up the battery, a component associated with the growth of the SEI, a term linked to the charge transfer processes during lithium intercalation and deintercalation, and a contribution related to the diffusion of lithium ions within the electrodes and electrolyte. In this paper, GEIS was used to derive the resistance contributions by fitting the impedance model presented in the next section. For the analysis of this paper a 10 Ah $LiCoO_2$ pouch cell (model 8773160K) manufactured by General Electronics Battery Co. Ltd was used [26]. This cell operates within a voltage range of 2.75 V to 4.2 V and can handle a maximum discharge current of 100 A (10C). In the following sections, the battery model used to fit the spectroscopy data, as well as the experimental setup and procedure, are described.

A. Battery impedance model

The impedance model used to interpret the results of GEIS consists of a series arrangement of the ohmic resistance (R_{HF}); an RC branch associated with the SEI layer (C_{SEI}, R_{SEI}); another RC branch representing the charge transfer resistance (R_{ct}) and the double-layer capacitance (C_{dl}); and an impedance element related to lithium-ion diffusion, known as the Warburg impedance (Z_W).

The impedance model and the resulting Nyquist plot are shown in Fig. 1. This paper focuses on estimating the low-frequency resistance of LiBs based on the high-frequency resistance, which was evaluated under various SOC levels, temperatures, and aging conditions. Specifically, the high-frequency resistance was determined from the intersection of the battery's response with the real axis. Physically, the low-frequency resistance (R_{LF}) should be considered as the sum of all four resistance components. However, accurately determining the diffusion resistance requires GEIS measurements at very low frequencies, which are challenging due to the long measurement times involved and the possibility that the total charge exchanged with the battery might shift the SOC outside the intended range. This could introduce nonlinear

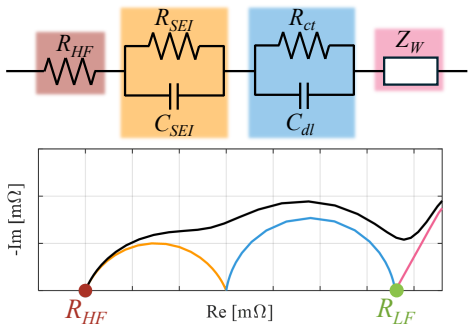

Fig. 1. Battery impedance model and corresponding Nyquist Plot.

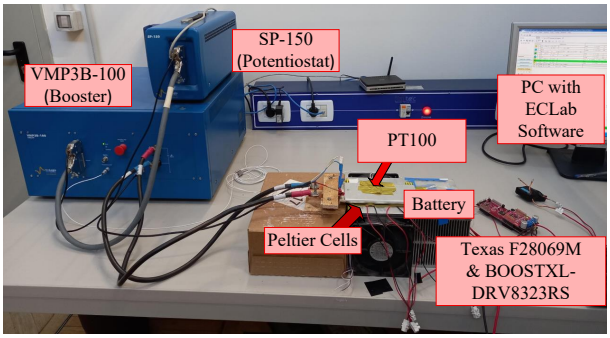

Fig. 2. Experimental setup.

effects that may distort the results. On the other hand, the time constant relevant for analyzing power fade can be related to the high frequency resistance, the SEI resistance, and the charge transfer one [27]; therefore, the R_{LF} considered in this paper was calculated as in (1):

$$R_{LF} = R_{HF} + R_{SEI} + R_{ct}. \tag{1}$$

R_{HF} and R_{LF} in the Nyquist diagram are shown in Fig. 1.

B. Experimental Setup and Test Procedure

The tests were conducted using a potentiostat (SP-150) paired with a booster (VMP3B-100) from Biologic Science Instruments, both managed through EC-Lab software on a PC connected via Ethernet. To maintain a constant battery temperature during testing, three Peltier cells connected in series were placed beneath the battery and mounted on a heatsink. The current through the Peltier cells was regulated by a Texas Instruments BOOSTXL-DRV8323RS converter [28], which was controlled by an F28069M controller board [29] using a proportional-integral regulator. The control system monitored the battery temperature via a PT100 sensor and adjusted the current through the Peltier cells to keep the battery temperature close to the target value. Although the Peltier cells were only on one side of the battery, the thin profile of the cell minimized any temperature gradient across it. Fig. 2 shows the experimental setup.

The test procedure was divided into two phases: resistance evaluation and aging cycling. The aging phase consisted of repeated charge and discharge cycles at a constant temperature of 30 °C and a constant current of 50 A (5C). Charging and discharging were limited between 20% and 80% of SOC and 3.45–4.05 V. The battery aging was quantified using the total moved charge Q measured in Ah and calculated as follows:

$$Q = \frac{1}{3600} \int_0^t |I_b| \, d\tau \tag{2}$$

where I_b is the battery current. Each aging cycle continued until a total charge throughput of about 5000 Ah was reached.

Resistance measurements were taken at the beginning of life and after each aging phase and were performed at eight different temperatures (20.0 °C, 22.5 °C, 25.0 °C, 27.5 °C, 30.0 °C, 33.5 °C, 38.0 °C, and 46.0 °C) and five different SOC levels (0%, 25%, 50%, 75%, and 100%). At each temperature, the battery was first charged using a constant current–constant voltage protocol at 10 A (1C) until the maximum cutoff voltage of 4.2 V was reached. The voltage was then held at 4.2 V until the current dropped to 100 mA (0.01C). After charging, the battery was allowed to rest for 1 hour, and then a GEIS measurement was performed from 10 kHz to 100 mHz with an amplitude of 300 mA (0.3C). The battery was then discharged at a constant current of 1C to reach 75% of SOC. At this SOC, after 1 hour of rest, another GEIS measurement was performed. This procedure was repeated, discharging the battery by 25% of SOC increments down to 0% of SOC. After the resistances at 0% of SOC were measured, the reference temperature was changed. The cell was recharged to 100% of SOC, and the procedure was repeated for the next target temperature.

III. Model Description

Neural networks are universal function approximators capable of modeling complex nonlinear relationships with high accuracy [30]. They have demonstrated strong performance across various domains, including computer science, finance, and engineering [31], [32]. Unlike other ML methods, NNs can predict system outputs without requiring explicit analytical models, offer notable computational efficiency [32], and high potential for parallelization and scalability [33]. Given these strengths, this study focuses on NNs as an efficient tool for addressing nonlinear estimation problems. In addition to all these reasons, in [34] we had already demonstrated that NNs were capable of obtaining good prediction results on a dataset very similar to the one used here.

This Section is organized as follows: Section III-A outlines the design choices made for the NN used in this work, and subsequently describes the training, validation, and testing pipeline; Section III-B presents the ensemble procedure adopted to enhance the robustness of the predictions generated by the previously introduced NN.

A. Neural Network design

The main challenge of this dataset lies in its limited size: 160 samples for training, 40 for testing, and only 4 available features (T, SOC, Q, and R_{HF}). Therefore, the NN must be

designed with careful consideration of the trade-off between model complexity and generalization. A network that is too simple may lack the accuracy needed, while an overly complex one is prone to overfitting due to the small size of the training set.

Preliminary experiments were conducted to select a proper NN architecture; for these tests a conventional 4-fold cross-validation strategy was used to train the NN models, where each fold contained 40 samples and was randomly generated with uniform distribution. The network that achieved excellent results on a similar dataset in our previous work [34] was used as a starting point. However, tests performed on the current data yielded poor accuracy, indicating that this dataset is more challenging than the previous one. For this reason, we decided to design a slightly more sophisticated network architecture. After conducting several tests, by adding more layers, more units, changing the batch size, the learning rate and/or modifying the activation functions to the previous network [34], we observed that the greatest improvement in performance was linked to adding an additional hidden layer. Tuning other parameters either worsened the performance or caused only negligible fluctuations. Introducing a second layer of units and adopting a pyramidal network structure significantly improved the predictive capabilities of the model. The resulting model employed in the experiments is summarized in Table I. Compared to the network used in our previous work [34], the current model increases the number of parameters from 26 to 209, when dealing with an input with three features. The fact that performance improves with this new network—which is a natural evolution of the previous one—confirms that the ML approach we are using is informative for the problem we are addressing.

TABLE I
NN ARCHITECTURE

Number of layers	3
Number of units in the first hidden layer	16
Number of units in the second hidden layer	8
Number of units in the output layer	1
Activation function of the hidden units	softmax
Activation function of the output unit	None
Data scaling	Standard Scaler
Loss function	MSE
Optimizer	Adam
Initial learning rate	$5 \cdot 10^{-3}$
Batch size	32

B. Bagging

Bagging (Bootstrap Aggregating) is a widely used ensemble learning method that aims to reduce the variance of predictive models by training multiple base learners on different subsets of the training data and aggregating their outputs. In the context of NNs for regression, each model in the ensemble is trained independently on a different bootstrap sample—a dataset generated by sampling with replacement from the original training set.

This approach introduces diversity among the models and helps mitigate overfitting, especially when working with small or noisy datasets. The final prediction is obtained by averaging the outputs of the individual networks, which typically results in more stable and accurate predictions compared to any single model.

Given the limited size of our dataset, we decided to perform bagging, thus aggregating multiple models to enhance robustness. In contrast to our previous work, where we used an ensemble of 100 lightweight NNs, the current architecture is larger and more computationally expensive. Therefore, we limited the ensemble to 20 models, balancing predictive performance and training cost. Following a standard bagging procedure, each one of these 20 models was trained using 160 data points sampled uniformly at random with repetitions from the original training set.

IV. MODEL PERFORMANCE

All the experiments were conducted on a workstation equipped with a 12th Gen Intel® Core™ i7-1255U CPU (base clock 1.7 GHz), 32 GB of RAM, and no dedicated GPU. Python was used as a programming language, with the Tensorflow library for the ML procedures.

Initially, we chose to focus exclusively on the new data introduced in this work with respect to [34], namely the measurements related to R_{LF}. Our objective was to develop an NN capable of predicting the R_{LF} resistance values under varying conditions of SOC, temperature T, and moved charge Q. In this initial phase of experimentation, we chose to exclude the feature measurements R_{HF}—used as the target variable in our previous work—in order to concentrate solely on the R_{LF} behavior.

Specifically, the network described in Section III-A was trained on R_{LF} measurements collected across all available SOC levels, temperatures, and moved charge values, with the exception of the moved charge value $Q = 20$ kAh. The prediction of R_{LF} values for all curves corresponding to $Q = 20$ kAh constituted the goal of our first experiment. These prediction results are shown in Figure 3, together with the experimental data, obtained as explained in Section II.

The results shown in Figure 3 are quite good, especially because they show that the model is able to clearly identify the correct trend of the 20 kAh curves, without having seen any of them before. To better quantify the performances of the model we computed the relative error for a given temperature and SOC, defined as follows:

$$\epsilon(\text{SOC}, T) \triangleq \frac{R_{LF}(\text{SOC}, T) - \hat{R}_{LF}(\text{SOC}, T)}{R_{LF}(\text{SOC}, T)}, \qquad (3)$$

where $\hat{R}_{LF}$ is the estimated value of resistance generated by the NN. We obtained an average value of this relative error equal to 0.7%, while the 95$^{\text{th}}$ percentile value is between -7.5% and 12.9%. This is a significant result, taking into account the small values of the resistance to be measured and the impedance measurement device's accuracy class of 1%.

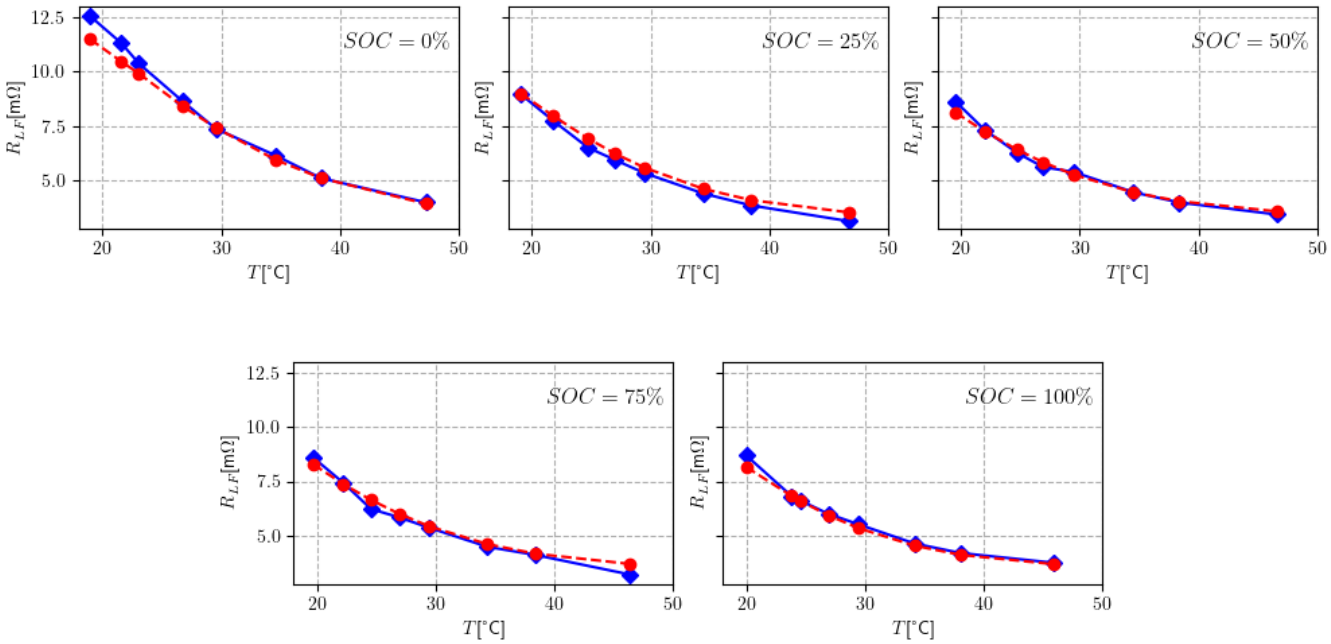

Fig. 3. Blue line: measured data points. Red line: estimated data points. The plots show the values at different SOC levels for the R_{LF} with $Q = 20$ kAh.

TABLE II
NRMSE OVER DIFFERENT SOC LEVELS FOR THE PREDICTIONS OF R_{LF} WITH $Q = 20$ KAH

SOC [%]	0	25	50	75	100
NRMSE [%]	5.96	4.71	3.66	4.49	3.43

TABLE III
NRMSE OVER DIFFERENT SOC LEVELS FOR THE PREDICTIONS OF R_{HF} WITH $Q = 20$ KAH, FROM PREVIOUS WORK [34]

SOC [%]	0	25	50	75	100
NRMSE [%]	1.57	1.72	2.52	2.83	3.38

To better quantify the prediction results, we also computed the Normalized Root Mean Square Error (NRMSE) for each SOC level. The definition of NRMSE is provided below:

$$\text{NRMSE (SOC)} \triangleq \sqrt{\frac{\sum_T \left(R_{LF}(\text{SOC},T) - \hat{R}_{LF}(\text{SOC},T)\right)^2}{\sum_T R_{LF}^2(\text{SOC},T)}}, \tag{4}$$

and the results are shown in Table II.

Comparing these results with those, reported in Table III, from the previous work [34] on a similar problem—the estimation of R_{HF}—it can be observed that the estimation of the R_{LF} resistance in this work—using an NN even more sophisticated than the previous one—is a more challenging problem than the previous one.

To investigate whether high-frequency measurements can improve low-frequency estimation, the NN model was re-trained from scratch on the same task, incorporating now R_{HF} as an additional input feature. The NRMSE results for this new setup are presented in Table IV, and are significant lower than those in Table II, and better than those in Table III too.

TABLE IV
NRMSE OVER DIFFERENT SOC LEVELS FOR THE PREDICTIONS OF R_{LF} WITH $Q = 20$ KAH, WHEN THE ADDITIONAL FEATURE R_{HF} IS CONSIDERED IN THE ML MODEL

SOC [%]	0	25	50	75	100
NRMSE [%]	7.18	1.22	2.35	2.03	1.74

Excluding SOC = 0%, predictions in Table IV show marked improvement with respect to those in Table II, with all NRMSE values below 3%. These findings demonstrate the network ability to effectively exploit the information contained in the R_{HF} feature to predict the target variable R_{LF}. The notable degradation in performance at SOC = 0% is likely due to the scarcity of training samples for this state, coupled with a possible presence of measurement noise within the limited dataset. By taking into consideration the additional feature R_{HF}, the average value of the relative error is equal to -1.3%, with the 95$^{\text{th}}$ percentile value between -8.6% and 4.2%. As a final remark, we want highlight that if we exclude the data points with SOC equal to 0% from the calculations, then the average relative error improves by around 82.4% when also using the additional R_{HF} feature in the ML model.

V. CONCLUSION

This work presented an ML approach for estimating the low-frequency resistance, R_{LF}, of LiBs, building upon previous research focused on high-frequency resistance, R_{HF}. Compared to prior studies, the estimation of R_{LF} proved to be a more challenging task due to its higher sensitivity to operating

conditions and limited data availability. To enhance model performance, R_{HF} was introduced as an additional input feature in the neural network. The results demonstrate that incorporating R_{HF} significantly improves the accuracy of R_{LF} predictions, with all NRMSE values falling below 3%, except at SOC = 0%, where performance is limited by data sparsity and possible measurement noise. Notably, excluding SOC = 0% data points leads to an 82.4% improvement in average relative error, highlighting the effectiveness of leveraging high-frequency information in low-frequency resistance estimation. These findings suggest that the proposed ML model, enhanced by R_{HF}, offers a practical and accurate solution for real-time battery resistance monitoring, especially under conditions well represented in the training dataset.

REFERENCES

[1] H. Deng and K. E. Aifantis, "Applications of lithium batteries," *John Wiley & Sons, Ltd*, pp. 83–103, 2023.

[2] N. Gupta, N. Kaur, S. K. Jain, and K. Singh Joshal, "Chapter 3 - smart grid power system," *Advances in Smart Grid Power System*, pp. 47–71, 2021.

[3] I. Bloom, B. Cole, J. Sohn, S. Jones, E. Polzin, V. Battaglia, G. Henriksen, C. Motloch, R. Richardson, T. Unkelhaeuser, D. Ingersoll, and H. Case, "An accelerated calendar and cycle life study of li-ion cells," *Journal of Power Sources*, vol. 101, no. 2, pp. 238–247, 2001.

[4] P. Shen, M. Ouyang, L. Lu, J. Li, and X. Feng, "The co-estimation of state of charge, state of health, and state of function for lithium-ion batteries in electric vehicles," *IEEE Transactions on Vehicular Technology*, vol. 67, no. 1, pp. 92–103, 2018.

[5] A. Farmann and D. U. Sauer, "A comprehensive review of on-board state-of-available-power prediction techniques for lithium-ion batteries in electric vehicles," *Journal of Power Sources*, vol. 329, pp. 123–137, 2016.

[6] L. Chen, M. Zhang, Y. Ding, S. Wu, Y. Li, G. Liang, H. Li, and H. Pan, "Estimation the internal resistance of lithium-ion-battery using a multi-factor dynamic internal resistance model with an error compensation strategy," *Energy Reports*, vol. 7, pp. 3050–3059, 2021.

[7] S. Lv, X. Wang, W. Lu, J. Zhang, and H. Ni, "The influence of temperature on the capacity of lithium ion batteries with different anodes," *Energies*, vol. 15, no. 1, 2022.

[8] Y. Bao, W. Dong, and D. Wang, "Online internal resistance measurement application in lithium ion battery capacity and state of charge estimation," *Energies*, vol. 11, no. 5, 2018.

[9] D. Anseán, V. García, M. González, J. Viera, C. Blanco, and J. Antuña, "Dc internal resistance during charge: Analysis and study on lifepo4 batteries," *2013 World Electric Vehicle Symposium and Exhibition (EVS27)*, pp. 1–11, 2013.

[10] M. Ecker, J. B. Gerschler, J. Vogel, S. Käbitz, F. Hust, P. Dechent, and D. U. Sauer, "Development of a lifetime prediction model for lithium-ion batteries based on extended accelerated aging test data," *Journal of Power Sources*, vol. 215, pp. 248–257, 2012.

[11] D.-I. Stroe, M. Swierczynski, S. K. Kær, and R. Teodorescu, "Degradation behavior of lithium-ion batteries during calendar ageing—the case of the internal resistance increase," *IEEE Transactions on Industry Applications*, vol. 54, no. 1, pp. 517–525, 2018.

[12] S. Barcellona, S. Colnago, G. Dotelli, S. Latorrata, and L. Piegari, "Aging effect on the variation of li-ion battery resistance as function of temperature and state of charge," *Journal of Energy Storage*, vol. 50, p. 104658, 2022.

[13] S. Skoog and S. David, "Parameterization of linear equivalent circuit models over wide temperature and soc spans for automotive lithium-ion cells using electrochemical impedance spectroscopy," *Journal of Energy Storage*, vol. 14, pp. 39–48, 2017.

[14] B. Ratnakumar, M. Smart, L. Whitcanack, and R. Ewell, "The impedance characteristics of mars exploration rover li-ion batteries," *Journal of Power Sources*, vol. 159, no. 2, pp. 1428–1439, 2006.

[15] S. Hossain Ahmed, X. Kang, and S. O. Bade Shrestha, "Effects of temperature on internal resistances of lithium-ion batteries," *Journal of Energy Resources Technology*, vol. 137, no. 3, p. 031901, 2015.

[16] H. Rauf, M. Khalid, and N. Arshad, "Machine learning in state of health and remaining useful life estimation: Theoretical and technological development in battery degradation modelling," *Renewable and Sustainable Energy Reviews*, vol. 156, p. 111903, 2022.

[17] H. Wang, D. Zhao, Y. Cai, Q. Meng, and G. P. Ong, "A trajectory-based energy consumption estimation method considering battery degradation for an urban electric vehicle network," *Transportation Research Part D: Transport and Environment*, vol. 74, pp. 142–153, 2019.

[18] A. Barré, B. Deguilhem, S. Grolleau, M. Gérard, F. Suard, and D. Riu, "A review on lithium-ion battery ageing mechanisms and estimations for automotive applications," *Journal of Power Sources*, vol. 241, pp. 680–689, 2013.

[19] S. Pelletier, O. Jabali, G. Laporte, and M. Veneroni, "Battery degradation and behaviour for electric vehicles: Review and numerical analyses of several models," *Transportation Research Part B: Methodological*, vol. 103, pp. 158–187, 2017.

[20] A. Nuhic, T. Terzimehic, T. Soczka-Guth, M. Buchholz, and K. Dietmayer, "Health diagnosis and remaining useful life prognostics of lithium-ion batteries using data-driven methods," *Journal of Power Sources*, vol. 239, pp. 680–688, 2013.

[21] Y. Li, K. Liu, A. M. Foley, A. Zülke, M. Berecibar, E. Nanini-Maury, J. Van Mierlo, and H. E. Hoster, "Data-driven health estimation and lifetime prediction of lithium-ion batteries: A review," *Renewable and Sustainable Energy Reviews*, vol. 113, p. 109254, 2019.

[22] M. Lin, C. Yan, W. Wang, G. Dong, J. Meng, and J. Wu, "A data-driven approach for estimating state-of-health of lithium-ion batteries considering internal resistance," *Energy*, vol. 277, p. 127675, 2023.

[23] M. A. Hoque, P. Nurmi, A. Kumar, S. Varjonen, J. Song, M. G. Pecht, and S. Tarkoma, "Data driven analysis of lithium-ion battery internal resistance towards reliable state of health prediction," *Journal of Power Sources*, vol. 513, p. 230519, 2021.

[24] X. Tan, D. Zhan, P. Lyu, J. Rao, and Y. Fan, "Online state-of-health estimation of lithium-ion battery based on dynamic parameter identification at multi timescale and support vector regression," *Journal of Power Sources*, vol. 484, p. 229233, 2021.

[25] C. Nguyen Van and D. T. Quang, "Estimation of soh and internal resistances of lithium ion battery based on lstm network," *International Journal of Electrochemical Science*, vol. 18, no. 6, p. 100166, 2023.

[26] "Lithium-ion battery datasheet." https://www.alibaba.com/product-detail/High-Rate-Discharge-Lithium-Polymer-8773160_1600182850317.html?spm=a2700.shop_plgr.41413.72.212e7121Bp84y4. Accessed: 2025-07-10.

[27] W. Waag, S. Käbitz, and D. U. Sauer, "Experimental investigation of the lithium-ion battery impedance characteristic at various conditions and aging states and its influence on the application," *Applied Energy*, vol. 102, pp. 885–897, 2013.

[28] "BOOSTXL-DRV8323RS converter." https://www.ti.com/tool/BOOSTXL-DRV8323RS. Accessed: 2025-07-10.

[29] "LAUNCHXL-F28069M control board." https://www.ti.com/tool/LAUNCHXL-F28069M. Accessed: 2025-07-10.

[30] S. Haykin, "Neural networks: a comprehensive foundation," *Prentice Hall PTR*, 1994.

[31] D. Silver, A. Huang, C. J. Maddison, A. Guez, L. Sifre, G. Van Den Driessche, J. Schrittwieser, I. Antonoglou, V. Panneershelvam, M. Lanctot, S. Dieleman, D. Grewe, J. Nham, N. Kalchbrenner, I. Sutskever, T. Lillicrap, M. Leach, K. Kavukcuoglu, T. Graepel, and D. Hassabis, "Mastering the game of go with deep neural networks and tree search," *nature*, vol. 529, no. 7587, pp. 484–489, 2016.

[32] M. Capra, B. Bussolino, A. Marchisio, G. Masera, M. Martina, and M. Shafique, "Hardware and software optimizations for accelerating deep neural networks: Survey of current trends, challenges, and the road ahead," *IEEE Access*, vol. 8, pp. 225134–225180, 2020.

[33] S. Lee, Q. Kang, R. Al-Bahrani, A. Agrawal, A. Choudhary, and W.-k. Liao, "Improving scalability of parallel cnn training by adaptively adjusting parameter update frequency," *Journal of Parallel and Distributed Computing*, vol. 159, pp. 10–23, 2022.

[34] S. Barcellona, L. Cannelli, S. Colnago, C. Laurano, and L. Piegari, "Cycle aging effect on lithium-ion battery resistance: a machine learning approach," *2023 IEEE International Conference on Metrology for eXtended Reality, Artificial Intelligence and Neural Engineering (MetroXRAINE)*, pp. 389–394, 2023.